Using redox-sensitive mitochondrial cytochrome Raman bands for label-free detection of mitochondrial dysfunction

Takeshi Morimoto[a†], Liang-da Chiu[b,c,†,*], Hiroyuki Kanda[a], Takeaki Ozawa[b], Makoto Nakamura[d], Kohji Nishida[e], Katsumasa Fujita[c,*], Takashi Fujikado[a]

[a]Department of Applied Visual Science, Osaka University Graduate School of Medicine, 2-2 Yamadaoka, Suita, Osaka 565-0871, Japan; [b]Department of Chemistry, the University of Tokyo, Graduate School of Science, 7-3-1 Hongo, Bunkyo-ku, Tokyo 113-0033 Japan; [c]Department of Applied Physics, Osaka University, Graduate School of Engineering, 2-1 Yamadaoka, Suita, Osaka 565-0871, Japan; [d]Department of Ophthalmology, Kobe University Graduate School of Medicine, Kobe, Japan; [e]Department of Ophthalmology, Osaka University Graduate School of Medicine, 2-2 Yamadaoka, Suita, Osaka 565-0871, Japan

Author contributions: T.M., L.-d. C., K.F., K.N., and T.F. designed research; T.M., L.-d. C., H.K., and K.F. performed research; T.O. participated in discussions and provided critical insights; M.N. contributed new reagents; T.M., L.-d. C., and K.F. analyzed data; and T.M., L.-d. C., K.F., and T.F. wrote the paper.

†Equal contribution

*Correspondence should be addressed to K. F. (fujita@ap.eng.osaka-u.ac.jp) or L.-d. C. (liang-da@chem.s.u-tokyo.ac.jp)

Keywords: Raman imaging, redox biology, mitochondria activity

Abstract

Mitochondrial activity is a widely used criterion to judge the metabolic condition of a living specimen. Numerous methods have been developed for related analysis, including the detection of O_2 consumption, trans-membrane potential, and ATP production. In this study, we demonstrate that the redox state of cytochromes can serve as a sensitive mitochondrial activity indicator in glutamate-stressed neuronal cells. Mitochondrial dysfunction was detected by Raman imaging as early as 30 min after glutamate-stressing. By comparing this result with other commonly used mitochondria function assays, we found Raman imaging has a similar sensitivity as ATP production and trans-membrane potential assays. Other viability tests, such as MTT assay and ROS production tests, showed a slower response than our method. A thorough understanding of cytochrome *c* dynamics with our new method will help establish Raman spectroscopy as a competitive clinical diagnosis tool for neurodegenerative diseases involving mitochondrial dysfunction.

Introduction

Mitochondria are known as the powerhouse of cells, which provides the necessary energy to maintain cellular functions through the production of ATP[1]. Mitochondria dysfunction not only influences the life and death decision at the cellular level[2], it also induces serious diseases at the organism level, including notorious neurodegenerative diseases such as Alzheimer's disease and Parkinson's disease[3]. Nowadays, a wide range of chemical indicators has been developed for the evaluation of mitochondria activity. Despite their success at the level of cellular studies, none of those methods could have further applications in clinical diagnosis since the chemical reagents required for those assays cannot be applied to human body. In this study, we introduce Raman spectroscopy as a label-free and non-destructive method to monitor mitochondrial activity. Raman spectroscopy has already been applied to observe the chemical state of various living specimen[4–8]. It is also demonstrated as a versatile clinical diagnostic tool with numerous successful reports on the detection of cancerous tissues in human patients[9–11]. Therefore, if Raman spectroscopy could be demonstrated as a reliable analytical tool to probe mitochondrial activity in living cells, it would not only contribute to the efficient and pretreatment-free analysis of cellular mitochondria function, it will also have the potential to be applied for the early detection of mitochondrial dysfunction for clinical purposes.

As mentioned above, one of the key functions of mitochondria that is essential to the maintenance of life is ATP production through oxidative phosphorylation (OXPHOS)[12]. OXPHOS starts with the respiratory electron transport chain (ETC) transferring electrons originating from NADH and succinate through four protein complexes (complex I ~ IV) with the help of ubiquinone and cytochrome *c*. During the electron transfer process, a proton gradient is generated across the inner mitochondrial membrane, which in turn drives ATP synthase to synthesize ATP[13]. A wide range of mitochondrial activity or cell viability assays have been developed surrounding the above-mentioned OXPHOS process. One of the most widely used assays of this kind, MTT assay, was thought to indicate succinate dehydrogenase (complex II) activity in the respiratory ETC, although recent studies suggested other intracellular reductants such as NADH also contribute to the conversion of MTT substrate into the detected formazan product[14]. ATP assay kits can also be easily found on the market and is already used to indicate cell viability in a wide range of schemes[15,16]. Different types of mitochondrial membrane potential probes are developed to visualize the proton gradient generated across the inner mitochondrial membrane during respiratory ETC by fluorescence microscopy[17,18]. Another less direct but also commercially available method to visualize mitochondrial activity is the monitoring of reactive oxygen species (ROS), a byproduct of the respiratory ETC with

important physiological roles in living organisms[19,20]. Unfortunately, despite the wide variety of methods to evaluate mitochondrial activity in living cells, all of them require the introduction of exogenous probes for detection, thus requires extra effort to modify those probes to be applied to human patients.

In the present study, we aim to establish the Raman spectroscopic observation of cytochrome redox state as a reliable mitochondrial activity indicator. Raman spectroscopy is one of the few label-free and non-invasive methods that can extract actual chemical information from living specimen. Although it is known to have weak signal intensity and is not suitable for the detection of a single type of chemical species in living specimen, by exploiting the resonance-enhancement effect of Raman scattering, this drawback can be mostly overcame[21]. Using 532 nm excitation light, the major cytochrome components in mitochondria, cytochrome *c* (cyt c) and cytochrome *b* (cyt b), could be selectively enhanced by such resonance-enhancement effect and can be clearly visualized by Raman imaging[22,23]. Cyt c is an essential electron carrier between the complex III and complex IV of the respiratory ETC[2], and cyt b is a component of the complex III that passes electrons to cyt c in the respiratory ETC. Therefore, the resonance-enhanced Raman spectroscopic detection of cytochrome redox state has the potential to serve as a sensitive mitochondrial OXPHOS activity indicator. However,

despite the numerous reports on the Raman spectroscopic redox quantification of cytochromes, especially cyt c, in living cells[22,24,25], the effectiveness of using their redox state to evaluate mitochondrial activity in living cells has yet to be discussed. The fact that both cyt c and cyt b are essential components of the respiratory ETC also makes it difficult to predict whether they would tend to reduce or oxidize when the ETC is disrupted. To properly address this issue, we systematically investigated how the Raman spectroscopic method respond to the glutamate induced neuronal cell death of an immortal retinal neuronal cell line, RGC-5, in comparison with the above-mentioned cell viability tests. Glutamate induced neuronal cell death is a common model for the study of oxidative stress-induced neuronal cell death associated with both acute and chronic neurological diseases and hypoxic insults, including amyotrophic lateral sclerosis, Parkinson's disease, Alzheimer's disease, glaucoma, and ischemic stroke[26–29]. Our results indicate that the cytochrome redox dynamics reported by Raman spectroscopy actually had a relatively good sensitivity to mitochondrial dysfunctions compared with many other assay methods.

Experimental

Cell cultures

The mouse immortalized RGC-5 cell line, which has been widely used as a cell culture

model to study the neurobiology of retinal neurons[30–32], was used in this study. Cells were cultured in 4500 mg/L D-glucose Gibco®DMEM (Life Technologies, Carlsbad, CA), 10% fetal bovine serum (FBS) (Biological Industries, Beit-Haemek, Israel), and 100 U/mL penicillin and 100 μg/mL streptomycin (Life Technologies) and were grown in a humidified atmosphere of 95% air and 5% CO_2 at 37°C.

Slit-scanning Raman Microscopy

All the hyperspectral Raman scattering images were obtained using a home-built slit-scanning Raman microscope with 532 nm excitation from a frequency-doubled Nd: YVO_4 laser (Verdi, Coherent Inc.). The laser beam is shaped into a line by a cylindrical lens and focused on the cells at the microscope stage by a 60X/1.27 NA water immersion objective lens（CFI Plan Apo IR 60XW, Nikon, Chiyoda, Japan). A line-shaped laser beam was formed using cylindrical lens sets and focused on the sample plane by the objective lens. The backscattered Raman signals from the cells are collected by the same objective lens, then pass into a spectrograph (MK-300, Bunkoh Keiki, Co, Ltd., Hachiohji, Japan) through a 532 nm long-pass edge filter (LP03-532RU-25, Semrock, Rochester, NY) and are then detected by a cooled Charge Coupled Device (CCD) camera (Pixis 400B, Princeton Instruments, Trenton, NJ). The Raman microscope was modified from the one reported in Palonpon et al[33]. The modified part is that we changed

the edge filters before the spectrometer to a notch filter[34].

Experimental Procedure of Raman imaging

Prior to Raman imaging, the cells were seeded on a quartz substrate (5 mm in diameter, 0.215 mm thick (Starbar Japan, Kobe, Japan) in 4500 mg/L D-glucose Gibco@DMEM, 10% FBS, and 100 U/mL penicillin and 100 μg/mL streptomycin and were grown in a humidified atmosphere of 95% air and 5% CO_2 at 37°C.

For Raman imaging, the culture medium was removed, and the cells were washed twice with Hepes-buffered Tyrode's solution composed of 150 mM NaCl, 10 mM glucose, 10 mM Hepes, 4.0 mM KCl, 1.0 mM $MgCl_2$, 1.0 mM $CaCl_2$, and 4.0 mM NaOH. The correction collar of the objective lens was set to 1.7 to compensate for the thickness of the quartz substrate. Raman scattering images were taken. All images were scanned for 40 steps within 20 μm width. The irradiated laser intensity at the sample plane and exposure time for each line was 2 mW/μm^2 and 1.5 s, respectively.

For reduction-oxidation experiment, the cells were observed by the Raman microscope at first, then cells were fixed by 4 wt% paraformaldehyde in 0.1 M phosphate buffered saline (PBS). 10 minutes after the fixation, the same cells were observed by the same microscope. After the second observation, 10 mM sodium dithionite (SDT) (Sigma-Aldrich, St Louis, MO) in 0.1M PBS was added to the medium. 10 minutes after the

administration of SDT, a strong reducing agent, the cells were observed again. Afterwards, 6.0 wt% H_2O_2 (Sigma-Aldrich, St.Louis, MO) in 0.1M PBS, a strong oxidizing agent, was added to the medium. Again, after 10 minutes, the same cells were observed for the fourth time.

For glutamate stressing experiment, cells were treated with 600 mM of L-glutamate (Sigma-Aldrich, St.Louis, MO) for 0.5, 1.0, 1.5 or 2.0 hours before Raman imaging.

Raman Data Analysis.

After measurement of Raman images, the Raman hyperspectral dataset was processed by singular value decomposition (SVD) for noise reduction, and we chose loading vectors that significantly contribute to the images contrast for the image[25,33]. Following SVD processing, the fluorescence background signal was subtracted from the Raman spectra at each pixel in the image by a modified polyfit fluorescence removal technique[25,33]. To evaluate the intensity of the Raman signals to reconstruct the Raman images, the Raman intensity at designated Raman shift was directly used. The Raman spectra displayed in each figure is averaged from a 5 pixel × 5 pixel area at arbitrary selected location where the 750 cm^{-1} cyt c contrast was strong. For Fig. 2 and Fig. 3, the Raman spectral image at different time points were concatenated into one dataset before SVD analysis in order to obtain better quantification results. All calculations were done by Matlab.

Immunocytochemical studies

To label the mitochondria in RGC-5 cells at different time points during glutamate treatment, control or treated cells were stained using 500 nM Mitotracker Red FM (Invitrogen) for 30 min at 37 °C, then fixed in 4.0 wt% PFA in PBS for 15 min, at 4 °C. After washes, cultures were pre-incubated with PBS containing 3.0 wt% Bovine serum albumin (BSA) for 60 min at room temperature, and incubated with primary antibody to cytochrome *c* (1:100, Invitrogen) overnight at 4 °C. After washes, cultures were incubated for 60 min with fluorescein isothiocyanate (FITC) conjugated Goat anti-mouse IgG (1:200, Invitrogen). Cells were examined with a fluorescence microscope EVOS FL Auto 2 Imaging System (ThermoFisher Scientific Inc) (FITC: Ex 490 nm / Em 525 nm; Mitotracker Red: Ex 579 nm / Em 599 nm).

Cell viability assay

Live RGC-5 cells were quantitated using Cell Proliferation Kit I (Roche Applied Science, Manheim, Germany). In brief, the cells were seeded at 1.0 x 10^4 cells/well in 96-well plates. Cell viability was assessed by the MTT (3-(4,5-Dimethylthiazol-2-yl)-2,5-diphenyltetrazolium bromide) assay. Cells were incubated with 500 mg of MTT and 0.27 mg of sodium succinate and allowed to react for 4 h at 37°C. The medium was removed and 1 ml of the solubilization reagent (0.01M HCl and 10 wt% SDS in DMSO (dimethyl

sulfoxide)) was added. Cell viability was measured at 550 nm in an ARVO plate reader (Perkin Elmer Japan Co., Ltd., Kanagawa, Japan). The results were expressed as mean percentage surviving cells relative to the number of control (untreated cells) as 100%. Each sample was assayed in sextuplicate.

Measurement of mitochondrial membrane potential

To measure the mitochondrial membrane potential, lipophilic cationic dye, 5,5',6,6'-tetrachloro-1,1',3,3'-tetraethylbenzimi-dazolylcarbocyanine iodide (JC-1) (Invitorogen) was used[38,39]. JC-1 spontaneously forms complexes known as J-aggregates with intense red fluorescence. On the other hand, in damaged cells with low mitochondrial membrane potential, JC-1 remains in the monomeric form, which shows only green fluorescence. RGC5 cells were seeded into 35 mm dishes at a density of 1.0 x 10^5 cells per dish. Then cells were loaded with JC-1 (2.0 μg/ml) for 30min at 37°C in culture medium containing 10 wt% FBS. Imaging of the cells with JC-1 were carried out before and at 30, 60, 90, 120 min after administration of glutamate using a fluorescence microscope EVOS FL Auto 2 Imaging System (ThermoFisher Scientific Inc). JC-1 fluorescence was monitored at 514 nm excitation/529 nm and 590 nm emission

Measurement of ATP

The level of intracellular ATP in cells was measured by using a ATP luminescence kit

(CA10, Toyo B-Net, Co.,LTD, Tokyo, Japan).

Briefly, cells (1.0 x 10^4 cells/ well) were lysed with 100 µl lysis buffer (Toyo ink, Tokyo, Japan) and centrifuged to pellet insoluble materials. The supernatant was added to a 96-well plate and followed by the addition of 100 µl of luciferin-luciferase solution (Toyo ink) to each well. Light emission was read using an ARVO plate reader. The ATP concentration was calculated based on a standard curve.

Measurement of Intracellular ROS

Intracellular ROS levels were measured with the OxiSelect™ Intracellular ROS Assay kit (Cell Biolabs, Inc., San Diego, CA)[40]. According to the manufacturing protocol, Cells (1.0×10^4 cells) were seeded on a black 96-well plate and incubated with 2', 7'-dichlorofluorescin diacetate (DCFH-DA) (1.0 mM) for the 60 min at 37°C and then washed in PBS. DCFH-DA is diffused into cells and deacetylated by cellular esterases to non-fluorescent 2', 7'-Dichlorodihydrofluorescin (DCFH). Then high concentration of glutamate (600mM) added into the culture. Oxidation of DCFH by ROS results in a fluorescent derivative 2',7'-dichlorofluorescein (DCF) whose fluorescence is proportional to the total ROS levels in the sample. Fluorescence was monitored at 492 nm excitation/535 nm emission using an ARVO plate reader. ROS levels were calculated by interpolation into a H_2O_2 standard curve.

Statistical analysis

Data are presented in box and whisker plots to describe the distribution of the data, and are analyzed statistically. For comparisons among three or more groups, one-way analysis of variance (ANOVA), followed by a Dunnett multiple-comparison test, was used. $P < 0.05$ was considered significant for all experiments.

Data availability

The data that support the findings of this study are available from the corresponding authors upon reasonable request.

Results & Discussion

Visualizing cytochrome redox state by the resonance enhanced Raman bands in RGC-5 cells

The Raman spectral imaging of RGC-5 using 532 nm excitation laser shows similar spectral image features with most reported cell lines (Fig. 1). A homogeneously distributed protein contrast throughout the cell can be given by the 1685 cm^{-1} amide I band shoulder (Fig. 1A). Lipid contrast that mostly depicts lipid droplets can be reconstructed by the 2850 cm^{-1} CH_2 stretch band (Fig. 1B). According to a previous report, the resonance-enhanced 750 cm^{-1} Raman band can be used to image reduced

cytochrome contrast that includes both reduced cyt c and cyt b in NCTC cells[22]. The 750 cm^{-1} contrast also resembles mitochondria distribution in RGC-5 cells, suggesting the 750 cm^{-1} band in RGC-5 and NCTC cells are of the same origin (Fig. 1C). We also confirmed that Raman images of RGC-5 cells using 589 nm laser do not show strong 750 cm^{-1} band (Sup. 1), further supporting the fact that the 750 cm^{-1} band we observed at 532 nm excitation is indeed the resonance-enhanced Raman band of cytochromes. According to the same report, it is possible to use the 600 cm-1 Raman band for the selective visualization of reduced cyt c[22]. In our study, the 600 cm^{-1} image also showed similar contrast to the 750 cm^{-1} image, both resembling mitochondria contrast (Fig. 1D). Unfortunately, since the 600 cm^{-1} Raman band overlaps with the Raman spectrum of the quartz substrate, the signal-to-noise ratio is worse than the 750 cm^{-1} image. Therefore, all following discussions will focus on the 750 cm^{-1} general cytochrome band. Although some other reports on the quantification of cytochrome redox in living cells assign the 1638 cm^{-1} band as the marker band for oxidized cytochromes[22,24], the 1638 cm^{-1} band is not always detectable in previous reports[25,34]. In this study, the RGC-5 Raman image constructed by the 1638 cm^{-1} signal also showed only a protein-like contrast like the amide I peak imaged at 1685 cm^{-1}, which does not resemble the cytochrome image constructed by the reduced cytochrome peak at 750 cm^{-1} at all (Fig. 1A, C, E). When

looking at the mitochondria Raman spectrum of the imaged cells, only at where the reduced cytochrome bands are the strongest, a barely visible bump at around 1638 cm^{-1} can be seen on top of the shoulder of the amide I band peaked at 1655 cm^{-1}. The 1638 cm^{-1} band becomes invisible at other locations where reduced cytochrome bands are still clearly visible (Fig. 1F). All these observations indicate that the concentration of oxidized cytochromes in control RGC-5 cells is too low for the 1638 cm^{-1} band to be constantly seen, thus the cytochrome redox state in RGC-5 cells can only be estimated by the intensity of the reduced cytochrome band alone.

To verify whether Raman spectral imaging can detect the redox state of cytochromes in RGC-5 cells, we obtained the Raman images of living and fixed RGC-5 cells, followed by fixed RGC-5 cells treated with sodium dithionite (SDT), a strong reducing agent, and H_2O_2, a strong oxidizing agent (Fig. 2). Previous studies already showed that fixed cells have weaker reduced cytochrome Raman bands[25]. Our study not only confirmed the same observation (Fig. 2A, B), but also took a further step to recover the 750 cm^{-1} cytochrome Raman signal *in situ* again by adding SDT to reduce the cytochrome in the fixed cells. As the result, the Raman images of the 750 cm^{-1} cytochrome band clearly showed an increase in intensity after SDT treatment (Fig. 2C). Since the 750 cm^{-1} Raman band is mostly contributed by the reduced form of cytochromes, this result proves that

the intensity reduction of the 750 cm^{-1} cytochrome Raman band after fixation is due to the oxidation of cytochromes, and indicates that Raman spectroscopy can indeed probe the reduction of cytochromes *in situ*. Following the reduction by SDT, we also confirmed that H_2O_2 treatment indeed resulted in the disappearance of reduced cytochrome bands, indicating that cytochrome oxidation can indeed be picked up *in situ* by Raman spectroscopy (Fig. 2D). The 600 cm^{-1} band that is specific to reduced cyt c showed exactly the same dynamics (E-H). Contrary to the reduced cytochrome Raman band, the amide I Raman signal at peaked at 1655 cm^{-1} remained unchanged throughout the experiment, suggesting that the addition of paraformaldehyde, SDT and H_2O_2 to the cells did not drastically change the protein structure in the cells (Fig. 2E-H).

The Raman spectra from the mitochondria rich region also showed respective enhancement and reduction of cytochrome intensity after SDT and H_2O_2 treatment (Fig. 2I). On the other hand, the nucleus spectra did not show much change across all experiments (Fig. 2J), further supporting our claim that the chemical treatments mainly influenced cytochrome behavior, and have much less effect to other components. The appearance of the strong 875 cm^{-1} H_2O_2 band after H_2O_2 treatment was observed in both cytochrome rich and nucleus spectra (Fig. 2I). These observations suggest that the cellular structures mostly survived the chemical treatments, and major chemical

composition difference at each experimental step is the redox environment within the cells. This is the first report of the chemical reduction of cytochromes visualized by Raman spectroscopy *in situ*. Previous studies have only used the weakening of the cytochrome Raman bands during H_2O_2 treatment as a proof of the redox sensitivity of resonance enhanced cytochrome Raman bands[24,25]. However, with only oxidation experiments, the possibility that cytochromes are simply degraded by H_2O_2 treatment instead of being oxidized cannot be ruled out. This reduction experiment convincingly demonstrates that Raman spectroscopy can indeed probe the redox state of cytochromes inside mammalian cells.

Raman spectral imaging of cytochromes in glutamate-stressed RGC-5 cells

Highly concentrated glutamate is known to damage neuronal cells[26,28]. Glutamate-stress leads to mitochondrial dysfunction and cell death, which is expected to induce changes in the cytochrome redox state. To verify whether such mitochondria dysfunction could be detected by Raman spectroscopy, we first took the Raman spectral images of RGC-5 cells at different time points before and after glutamate treatment (Fig. 3A-J). It is clear that the cytochrome Raman image has the highest contrast in the control image (Fig. 3A), and the contrast weakens as the glutamate treatment time becomes longer (Fig. 3B-E). The averaged Raman spectra from the cytoplasm also showed the similar

trend that the cytochrome peaks are the strongest at their control state, and quickly lost most of their intensity within 1 hour after glutamate treatment (Fig. 3F-J). This is very different from apoptosis, during which significant decrease of reduced cytochrome Raman bands was not observed even after cyt c is released from mitochondria to cytosol[25]. This difference in cytochrome redox dynamics during cell death is most likely due to the necrotic nature of glutamate-stress induced cell death. We also took the electron microscopy image of RGC-5 cells after different glutamate treatment times to confirm whether necrosis indeed occurred in our experimental condition (Fig. 4). As the result, most cells displayed morphological features of necrosis as soon as 30 min, such as swollen organelles with intact nuclei (Fig. 4B, G). After 1hr of glutamate treatment, cells showed an advanced stage of necrosis with total loss of the plasma membrane and severe mitochondria damage (Fig. 4C, H). The progression of necrotic cell death due to glutamate treatment can be further visualized by the images at 90 and 120 min (Fig. 4D ,E, I, J).

In order to further verify whether the weakening of the 750 cm^{-1} Raman band intensity is indeed due to the oxidation of cytochromes, not the rapid decrease of local cytochrome concentration, we also performed cyt c immunostaining throughout the glutamate-stress

experiment and compared its localization with mitochondria distribution (Fig. 5). The reason why only cyt c is chosen for immunostaining is because cyt c is known to dissipate into the cytosol during apoptosis, resulting in significant decrease in its local concentration[25]. Cyt b is a membrane protein, thus its local concentration is unlikely to change unless the mitochondrial structure is completely scattered into the cytosol[35]. It can be seen that despite the morphological change of RGC-5 cells over the 2-hour glutamate-induced cell death process, cyt c remained to co-localize with mitochondria (Fig. 5). Previous study has demonstrated that both fluorescence imaging[36] and Raman spectral imaging[25] are capable of visualizing the cyt c release process from mitochondria to cytosol. No such active release of cyt c can be observed by immunostaining in our glutamate-induced necrosis experiment, so the local concentration of cyt c is not likely to significantly decrease during glutamate-induced necrosis. Combining our Raman spectral imaging and immunostaining results, the oxidation of cytochromes in mitochondria is proved to be the major reason for the decrease in the 750 cm^{-1} Raman band intensity in glutamate-stressed RGC-5 cells.

Raman spectroscopy can detect mitochondrial dysfunction earlier than MTT assay

Since the reduced cytochrome Raman band at 750 cm^{-1} in RGC-5 cells is shown to be a reliable cytochrome redox indicator that reflects mitochondria activity during glutamate-

induced cell death, we systematically investigated the effectiveness of this method compared with other widely used mitochondria activity or cell viability indicators under the same scheme. Here, one determining advantage of Raman spectral imaging has already shown up, which is its capability of being able to analyze and image mitochondrial activity at sub-organelle level resolution. In order to fairly compare our Raman spectral imaging method with the other commonly used assays, we calculated the statistical behavior of reduced cytochrome Raman intensity during glutamate-induced cell death. The result showed a similar trend to the Raman images aforementioned, with a rapid drop of the 750 cm^{-1} Raman band intensity within 30 min ~ 1 hr after glutamate treatment (Fig. 6A). The study was a time-course experiment that measures different culture dishes at different time points. The number of cells chosen for the statistical analysis at each time-point was 56 cells for 0 min, 57 cells for 30 min, 45 cells for 60 min, 60 cells for 90 min, and 58 cells for 120 min. We also applied the same analysis to the other resonance enhanced cytochrome Raman bands, namely the 1127, 1313, and 1585 cm^{-1} bands (Fig. 6A). A rapid drop of Raman intensity within 30 min ~ 1 hr after glutamate treatment was also seen in all cytochrome related peaks. The result showed that Raman spectroscopy is capable of detecting mitochondrial dysfunction during glutamate-stressing within 30 min.

We further compared this result with the most widely used cell viability test, MTT assay. Similar to the Raman measurements, the MTT assay at different time-points were collected different wells in a plate, and the 2-hr time-course experiment was repeated for 7 times for statistical analysis. MTT assay also showed a decrease in cell viability from around 30 to 60 minutes after glutamate administration (Fig 6B). However, the response at the 30 min time point is obviously more ambiguous compared with our Raman spectroscopic method. This indicates that our method is more sensitive to mitochondrial function compared with MTT assay. The earlier detection of glutamate-stress by monitoring the cytochrome redox state is somewhat expected, because MTT assay evaluates cell viability through the reduction of MTT by the complex II in the respiratory ETC and NADH. Although complex II function is directly associated with mitochondrial function, NADH is mainly reduced from NAD^+ by the tricarboxylic acid (TCA) cycle or glycolysis[14]. Glutamate-stress is known to have a more direct impact to the OXPHOS system by depolarizing the mitochondrial membrane[28], so the NADH produced by TCA cycle and glycolysis would lead to a slower response for MTT assay to glutamate-stress. On the other hand, cytochromes are intermediate electron carriers in the respiratory ETC, so any disruption in the ETC would immediately be reflected by the cytochrome redox state.

Raman spectroscopy as a competent mitochondrial activity indicator

Beside MTT assay, we also compared our Raman spectroscopic method with other mitochondrial assays that targets more directly at the OXPHOS pathway. ATP assay directly quantifies ATP, the end product of the OXPHOS pathway, to evaluate mitochondrial activity[16]. Statistical analysis from 48 2-hr time-course experiments with different time-point conducted in different wells were performed. As the result, ATP assay also showed a quick drop of ATP concentration in RGC-5 cells between 30 min ~ 1 hr, which is at a very similar time-scale to the Raman spectroscopic observation of cytochrome oxidation (Fig. 6C). A significant decrease in the mitochondrial membrane potential generated by the respiratory ETC was also probed by JC-1 dye at both the 30 min and 1 hr time point (Fig. 6D), which also synchronizes with our Raman spectroscopic measurement (Fig. 3A-F). These observations showed for the first time that the Raman spectroscopic quantification of cytochrome redox state can indeed be used as a mitochondrial activity indicator. Cells with more intact OXPHOS activity tend to have a higher ratio of reduced cytochromes, while lost in OXPHOS activity due to glutamate-stress can lead to an increased proportion of oxidized cytochromes.

ROS generation is another commonly used parameter to evaluate impairments in the OXPHOS pathway. OXPHOS activity is known to produce ROS even under normal

conditions, and disruption of the OXPHOS pathway usually leads to an increased level of ROS generation[37]. We conducted 9 2-hr time-course ROS assays with different time-points in different wells for statistical analysis, and the result showed that ROS level in RGC-5 cells raised only after 1 hr of glutamate stress (Fig. 6E). The slower response of ROS assay compared with other OXPHOS activity indicators, including our Raman spectroscopic method, is most likely due to the fact that the antioxidant defense system that counters increased ROS level in cells[38] still remains active for a while even after mitochondrial activity is already damaged by the glutamate stress. These results suggest that mitochondrial dysfunction is a rather early stage process in glutamate-induced cell death compared with the dysregulation of other homeostasis maintaining processes, and Raman spectroscopy is able to catch the early sign of mitochondrial dysfunction in glutamate-stressed RGC-5 cells.

Conclusion

In the present study, we established Raman spectroscopy as a powerful method to detect mitochondrial dysfunction during glutamate-induced neuronal cell death, a commonly used model of etiology in many neurodegenerative diseases. We first demonstrated that Raman spectral imaging is indeed capable of visualizing cytochrome redox in fixed cells after both reductant treatment and oxidant treatment. The recovery

of cytochrome signal after cell fixation by reductant treatment *in situ* was observed for the first time in our experiment. The recovered cytochrome signal showed a slightly stronger cytochrome intensity as in living cells (Fig. 2). Our result clearly excluded the possibility that the decrease in cytochrome intensity after cell fixation is due to the degradation or redistribution of cytochromes, and the possibility that photobleach resulted in the cytochrome intensity drop.

By confirming that cytochrome distribution does not change in RGC-5 cells before and after glutamate treatment, we further revealed that cytochromes were almost completely oxidized within 1 hr during glutamate-induced cell death. The comparison of our Raman method with other mitochondrial activity assays proved that our method can detect mitochondrial dysfunctions faster than MTT assay and ROS assay, and performs similar to methods that directly visualize OXPHOS activity in mitochondria, such as ATP assay and mitochondrial membrane potential probes. The sub-cellular resolution of Raman spectral imaging also enabled further studies the activity of individual mitochondrion in living cells. Considering that mitochondrial dysfunction not only influences cellular behaviors, but also serves as an early stage symptom of many neurodegenerative diseases, the label-free nature of Raman spectroscopy brings advantage to the study of mitochondrial activity *in vivo*, and is expected to help the early diagnosis of those

diseases in patients.

One limitation of the current Raman detection method is that only the reduced cytochrome Raman bands is always observable. For example, we were not able to detect the oxidized cytochrome band in this study, so it was necessary to perform immunostaining experiments to make sure that cytochrome distribution indeed co-localized with mitochondria throughout the glutamate-induced cell death process. Since this study indicated that the 750 cm^{-1} cytochrome Raman band is strong at high OXPHOS activity, the 750 cm^{-1} Raman band intensity might serve as an optical mean to probe regional hypoxia in living specimen. Establishing methods that could constantly extract the weak oxidized cytochrome Raman band would further improve the usability of Raman spectroscopy to monitor mitochondrial activity. Also, specialized setups would need to be developed to apply Raman spectroscopic detection of living animals or human patients instead of microscopes. Still, confirming that the redox state of cytochromes can indeed be used to evaluate mitochondrial OXPHOS activity is already a significant step towards using Raman spectroscopy to detect neurodegenerative diseases at an early stage to improve the prognosis of such diseases.

Conflicts of interest

The authors declare no conflict of interest.

Acknowledgments

The authors would like to thank E.Suga for technical assistance with the experiments. This work was supported by grants from Asian CORE Program, Japan Society for the Promotion of Science (JSPS), Advanced Nano Photonics Research and Education Center in Asia, and KAKENHI including Grant-in-Aid for Scientific Research (C) (Grant no. 26462684,), Scientific Research (B) (Grant no. 25293354), Scientific Research (S) (Grant no. 26220805), and Specially Promoted Research (Grant no. 26000011).

References

1 J. Nunnari and A. Suomalainen, *Cell*, 2012, **148**, 1145–1159.

2 M. Hüttemann, P. Pecina, M. Rainbolt, T. H. Sanderson, V. E. Kagan, L. Samavati, J. W. Doan and I. Lee, *Mitochondrion*, 2011, **11**, 369–81.

3 M. H. Yan, X. Wang and X. Zhu, *Free Radic. Biol. Med.*, 2013, **62**, 90–101.

4 L. Chiu, S.-H. Ho, R. Shimada, N.-Q. Ren and T. Ozawa, *Biotechnol. Biofuels*, 2017, **10**, 9.

5 T. Huser and J. Chan, *Adv. Drug Deliv. Rev.*, 2015, **89**, 57–70.

6 C. Matthäus, C. Krafft, B. Dietzek, B. R. Brehm, S. Lorkowski and J. Popp, *Anal. Chem.*, 2012, **84**, 8549–56.

7 C.-K. Huang, M. Ando, H. Hamaguchi and S. Shigeto, *Anal. Chem.*, 2012, **84**, 5661–8.

8 T. Ichimura, L. Chiu, K. Fujita, H. Machiyama, T. Yamaguchi, T. M. Watanabe and H. Fujita, *Sci. Rep.*, 2016, **6**, 37562.

9 M. Jermyn, K. Mok, J. Mercier, J. Desroches, J. Pichette, K. Saint-arnaud, L. Bernstein, M. Guiot, K. Petrecca and F. Leblond, *Sci. Transl. Med.*, 2015, **7**, 1–10.

10 M. S. Bergholt, W. Zheng, K. Y. Ho, M. Teh, K. G. Yeoh, J. B. Y. So, A. Shabbir and Z. Huang, *J. Biophotonics*, 2013, **6**, 49–59.

11 A. S. Haka, K. E. Shafer-Peltier, M. Fitzmaurice, J. Crowe, R. R. Dasari and M. S. Feld, *Proc. Natl. Acad. Sci. U. S. A.*, 2005, **102**, 12371–6.

12 Y. Hatefi, *Annu. Rev. Biochem.*, 1985, **54**, 1015–1069.

13 F. Sun, Q. Zhou, X. Pang, Y. Xu and Z. Rao, *Curr. Opin. Struct. Biol.*, 2013, **23**, 526–538.

14 M. V. Berridge, P. M. Herst and A. S. Tan, in *Biotechnology annual review*, 2005, vol. 11, pp. 127–152.

15 G. Y. Lomakina, Y. A. Modestova and N. N. Ugarova, *Biochemistry*, 2015, **80**, 701–713.

16 R. Jitschin, A. D. Hofmann, H. Bruns, A. Giessl, J. Bricks, J. Berger, D. Saul, M. J. Eckart, A. Mackensen and D. Mougiakakos, *Blood*, 2014, **123**, 2663–2672.

17 M. Reers, S. T. Smiley, C. Mottola-Hartshorn, A. Chen, M. Lin and L. B. Chen, in *Methods Enzymol*, 1995, vol. 260, pp. 406–417.

18 S. Sakamuru, M. S. Attene-Ramos and M. Xia, 2016, vol. 1473, pp. 17–22.

19 J. M. Suski, M. Lebiedzinska, M. Bonora, P. Pinton, J. Duszynski and M. R. Wieckowski, in *Methods in Molecular Biology*, 2012, vol. 810, pp. 183–205.

20 J. Dan Dunn, L. A. J. Alvarez, X. Zhang and T. Soldati, *Redox Biol.*, 2015, **6**, 472–485.

21 L. Wei, Z. Chen, L. Shi, R. Long, A. V. Anzalone, L. Zhang, F. Hu, R. Yuste, V. W. Cornish and W. Min, *Nature*, 2017, **544**, 465–470.

22 M. Kakita, M. Okuno and H. Hamaguchi, *J. Biophotonics*, 2013, **6**, 256–259.

23 K. Hamada, K. Fujita, N. I. Smith, M. Kobayashi, Y. Inouye and S. Kawata, *J. Biomed. Opt.*, 2008, **13**, 044027.

24 N. A. Brazhe, M. Treiman, A. R. Brazhe, N. L. Find, G. V Maksimov and O. V Sosnovtseva, *PLoS One*, 2012, **7**, e41990.

25 M. Okada, N. I. Smith, A. F. Palonpon, H. Endo, S. Kawata, M. Sodeoka and K. Fujita, *Proc. Natl. Acad. Sci.*, 2012, **109**, 28–32.

26 J. Hugon, J. M. Vallat and M. Dumas, *Rev. Neurol. (Paris).*, 1996, **152**, 239–48.

27 M. Flint Beal, *Ann. Neurol.*, 1998, **44**, S110–S114.

28 Y. Wang and Z. Qin, *Apoptosis*, 2010, **15**, 1382–1402.

29 R. Sattler and M. Tymianski, *Mol. Neurobiol.*, 2001, **24**, 107–130.

30 C. J. Lieven, L. E. Millet, M. J. Hoegger and L. A. Levin, *Exp. Eye Res.*, 2007, **85**, 678–683.

31 N. J. Van Bergen, J. P. M. Wood, G. Chidlow, I. A. Trounce, R. J. Casson, W.-K. Ju, R. N. Weinreb and J. G. Crowston, *Investig. Opthalmology Vis. Sci.*, 2009, **50**, 4267.

32 A. F. Thompson, M. E. Crowe, C. J. Lieven and L. A. Levin, *PLoS One*, 2015, **10**, e0145270.

33 A. F. Palonpon, J. Ando, H. Yamakoshi, K. Dodo, M. Sodeoka, S. Kawata and K. Fujita, *Nat. Protoc.*, 2013, **8**, 677–692.

34 L. Chiu, T. Ichimura, T. Sekiya, H. Machiyama, T. Watanabe, H. Fujita, T. Ozawa and K. Fujita, *Sci. Rep.*, 2017, **7**, 43569.

35 M. D. Esposti, S. De Vries, M. Crimi, A. Ghelli, T. Patarnello and A. Meyer, *Biochim. Biophys. Acta - Bioenerg.*, 1993, **1143**, 243–271.

36 J. C. Goldstein, N. J. Waterhouse, P. Juin, G. I. Evan and D. R. Green, *Nat. Cell Biol.*, 2000, **2**, 156–62.

37 D. C. Liemburg-Apers, P. H. G. M. Willems, W. J. H. Koopman and S. Grefte, *Arch. Toxicol.*, 2015, **89**, 1209–1226.

38 P. D. Ray, B.-W. Huang and Y. Tsuji, *Cell. Signal.*, 2012, **24**, 981–990.

Figure legends

Fig.1 Raman spectral image of living RGC-5 cells

The Raman images of protein at the 1685 cm^{-1} amide I shoulder (A), lipid at 2850 cm^{-1} CH_2 stretch (B), reduced cytochromes at 750 cm^{-1} (C), reduced cyt c at 600 cm^{-1} (D), and oxidized cytochromes at 1638 cm^{-1} (E). The Raman spectra at where the reduced cytochromes are the strongest in the cells (black arrow in C) and where the reduced cytochromes are weaker (dotted arrow in C) are shown in the Raman spectra (F). The Raman bands selected to construct the images are labelled by the respective colors in the Raman spectra (F). The oxidized Raman band is so weak in RGC-5 cells that the band is barely seen in the spectra and the image contrast at 1638 cm^{-1} showed only protein. The width of images A-E is 20 μm.

Fig. 2. Raman spectral imaging of RGC-5 cells during cyt c redox state manipulation.

The 750 cm^{-1} Raman images of reduced cytochromes in the same RGC-5 cells before fixation (A), after fixation (B), after adding SDT, a strong reductant (C), and after adding H_2O_2, a strong oxidant (D). The protein contrast of the same RGC-5 cells at the respective states are also shown (E-H). The color scale between A-D and E-H are unified and comparable with each other. The 750 cm^{-1} Raman band apparently weakened after

fixation, strengthened after adding SDT, and weakened again after adding H_2O_2, while the protein contrast remained mostly unchanged (E-H). The mitochondria spectra of the imaged cells at each stage (I, spectra acquired from the indicated region in A-D) showed the same trend. The Raman spectra of cell nucleus at different stages (J) showed minor changes. The strong H_2O_2 band at 875 cm^{-1} in the Fixed + SDT + H_2O_2 spectra (I, J) is omitted to unify the vertical scale of each spectra. The Raman bands used to construct the Raman images in A-H is labelled in respective colors. The cytochrome spectra are obtained at the arrowed spot in the cytochrome image, and the nucleus spectra are obtained at the arrowed spot in the nucleus image. The width of all Raman images is 20 μm.

Fig.3 Raman spectral images of cytochromes in cells after the administration of highly concentrated glutamate.

The 750 cm^{-1} reduced cytochrome Raman images before (A), 30 min after (B), 60 min after (C), 90 min after (D), and 120 after (E) glutamate treatment. The color scale between A-E are unified and comparable with each other. The Raman spectra taken from the region indicated by the white arrows in A-E is shown in F-J respectively. The spectra were normalized according to the broad Raman band from the quartz substrate that

partially overlap with the 750 cm^{-1} band labelled in green. A clear drop in the 750 cm^{-1} band intensity can be seen from both the images (A-E) and the spectra (F-J). The width of all Raman images is 20 μm.

Fig. 4 Electron microscopy image of RGC-5 cells during cell death.

The electron microscope image of the different compartments of cells images before (A, F), 30 min after (B, G), 60 min after (C, H), 90 min after (D, I), and 120 min after (E, J) glutamate treatment. White arrows point out the swollen mitochondria. Scale bar, A-E 5 μm., F-J 500 nm

Fig. 5 Distribution of cyt c in RGC-5 cells during cell death.

The comparison of Mitotracker red staining (red images) and cyt c immunostaining (green images) throughout the glutamate-induced cell death process. The merged image showed good colocalization between cyt c immunostaining and mitochondria distribution. Scale bar, 25 μm.

Fig. 6 Comparing Raman spectroscopy with other mitochondria activity indicators.

The box plots showing the minimum, lower quartile, media, upper quartile and maximum intensity value of the reduced cytochrome Raman bands at 750, 1127, 1313, 1585 cm^{-1}

during glutamate-stressing (A) was compared with the box plots of MTT assay (B), ATP assay (C), mitochondrial membrane potential probes (D), and ROS assay (E). A clear decrease in cytochrome Raman band intensity was observed at the 30 min time point (A), with only MTT assay (B) and mitochondrial membrane potential probe (D) with similar sensitivity. Scale bar in D, 50 μm. The ∗ marks in (A), + marks in (B), † marks in (C), and ‡ mark in (E) represent that the data points has $P < 0.0001$ vs the 0 min data point calculated by one-way ANOVA followed by Dunnett test.,

Fig. 1

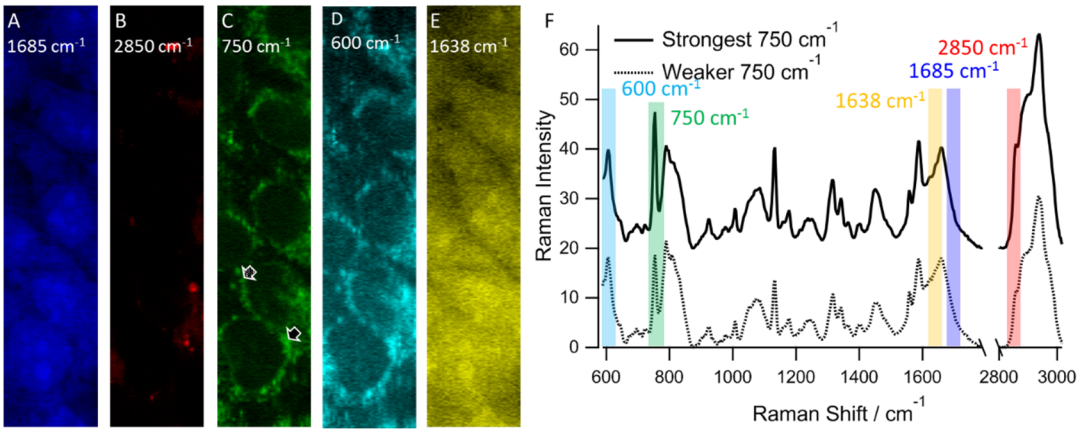
A
1685 cm-1
B
2850 cm-1
C
750 cm-1
D
600 cm-1
E
1638 cm-1
F
Strongest 750 cm-1
Weaker 750 cm-1
600 cm-1
750 cm-1
1638 cm-1
2850 cm-1
1685 cm-1
Raman Intensity
Raman Shift / cm-1
0
10
20
30
40
50
60
600
800
1000
1200
1400
1600
2800
3000

Fig. 2

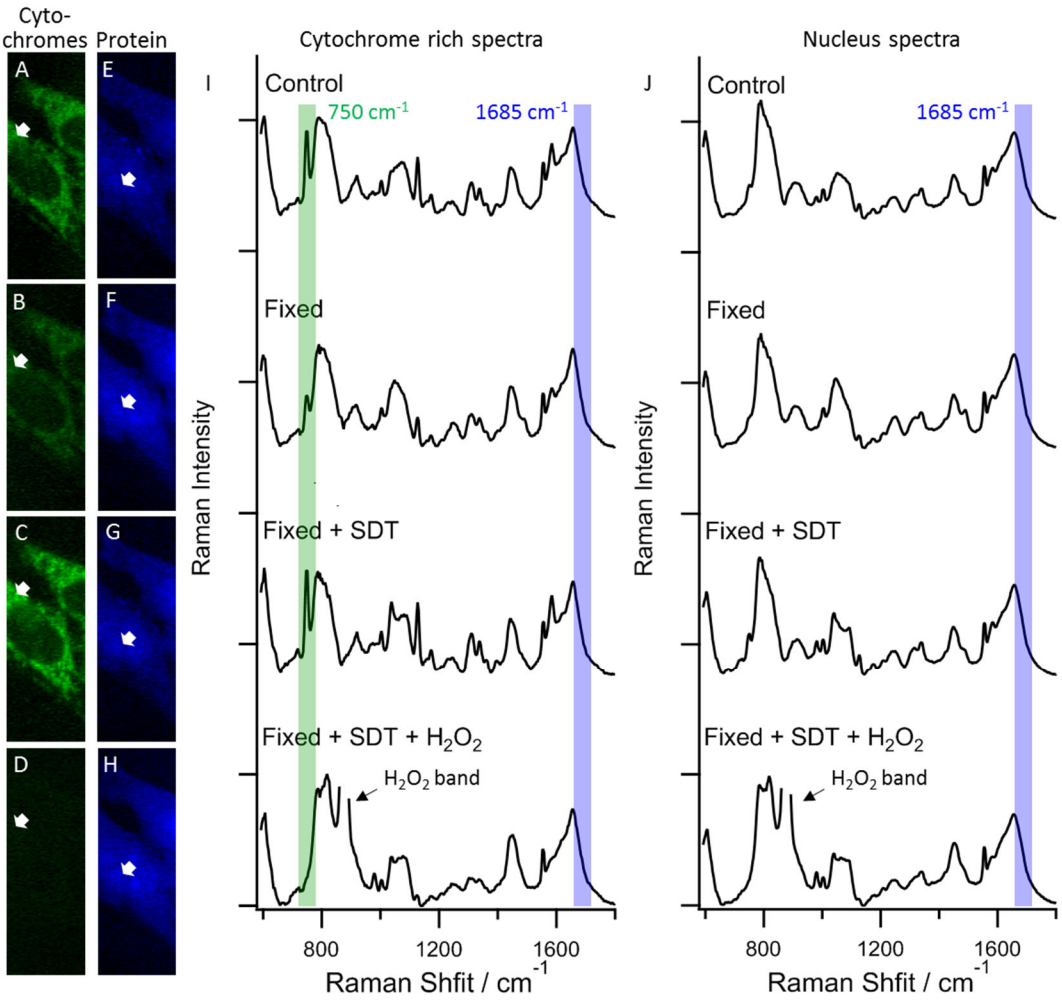
Cyto-
chromes
Protein
A
E
B
F
C
G
D
H
Cytochrome rich spectra
Nucleus spectra
I
J
Control
Fixed
Fixed + SDT
Fixed + SDT + H2O2
750 cm-1
1685 cm-1
H2O2 band
Raman Intensity
800
1200
1600
Raman Shfit / cm-1

Fig. 3

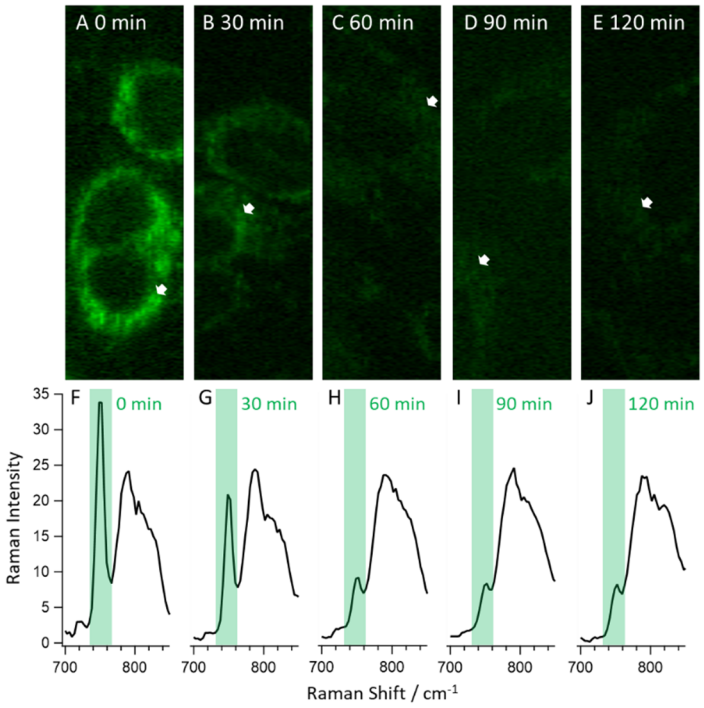
A 0 min
B 30 min
C 60 min
D 90 min
E 120 min
F 0 min
G 30 min
H 60 min
I 90 min
J 120 min
Raman Intensity
Raman Shift / cm-1

Fig. 4

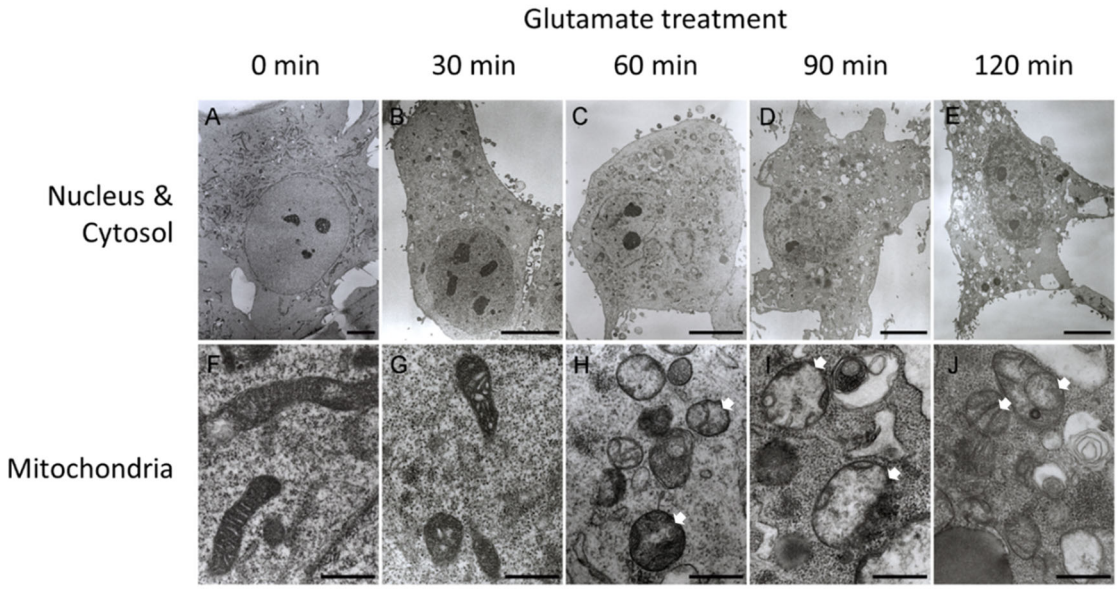
Glutamate treatment
0 min
30 min
60 min
90 min
120 min
Nucleus & Cytosol
Mitochondria
A
B
C
D
E
F
G
H
I
J

Fig. 5

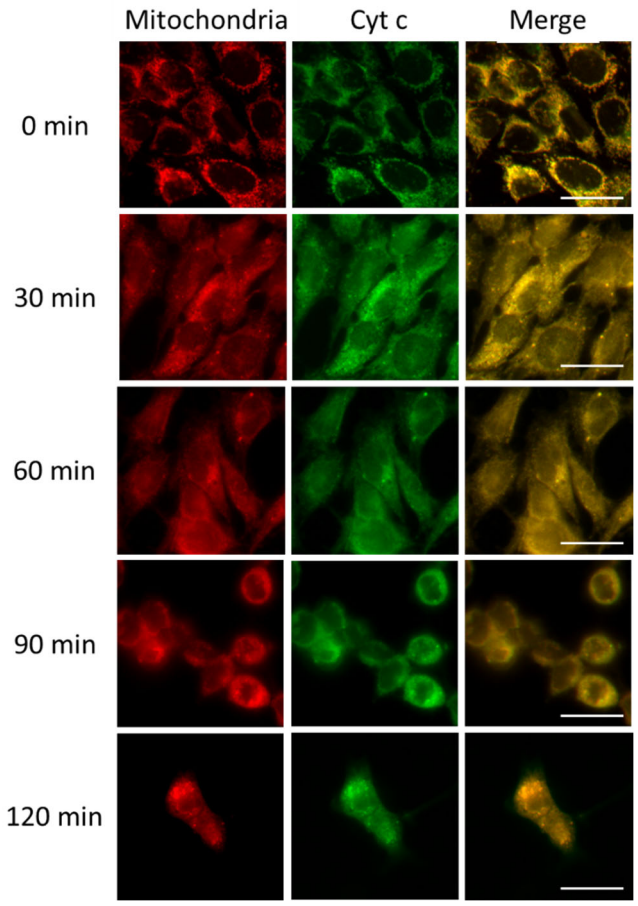

Fig. 6

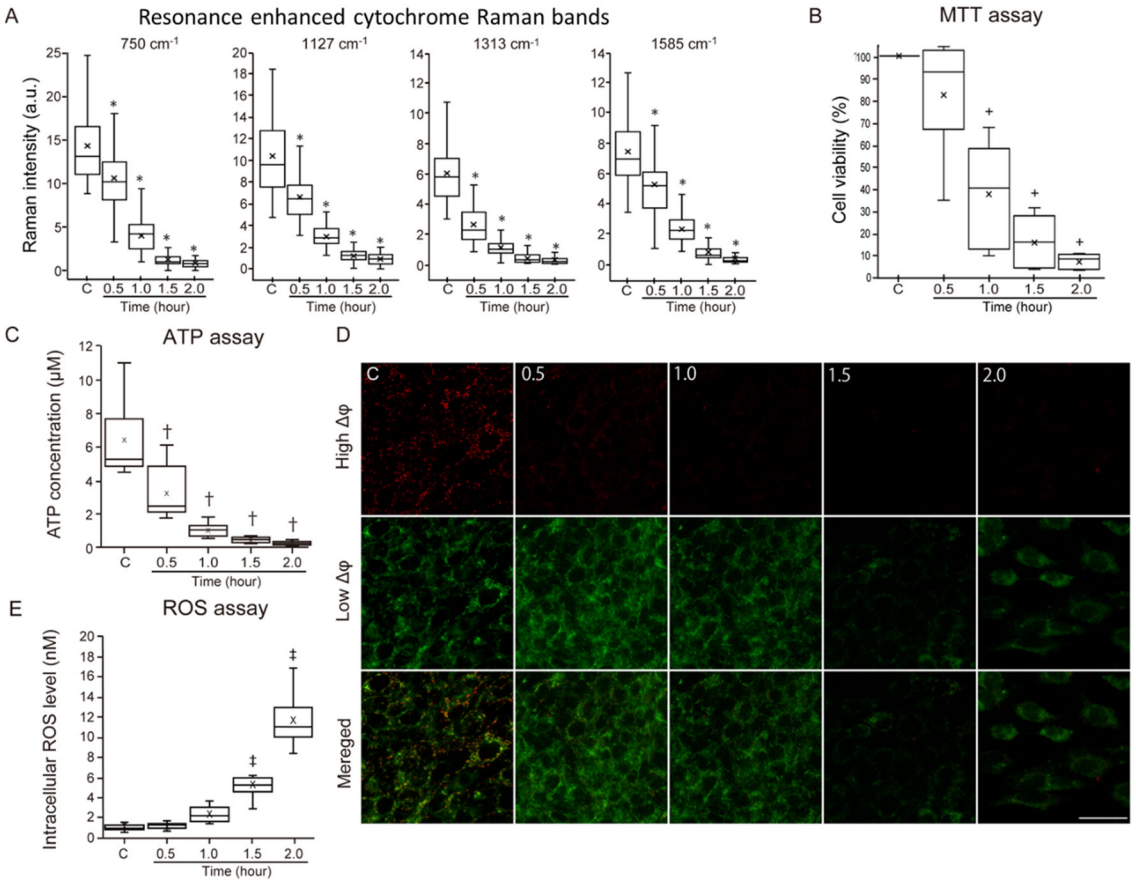
A
Resonance enhanced cytochrome Raman bands
750 cm-1
1127 cm-1
1313 cm-1
1585 cm-1
Raman intensity (a.u.)
C 0.5 1.0 1.5 2.0
Time (hour)
B
MTT assay
Cell viability (%)
C
ATP assay
ATP concentration (μM)
D
C
0.5
1.0
1.5
2.0
High Δφ
Low Δφ
Mereged
E
ROS assay
Intracellular ROS level (nM)

For TOC only

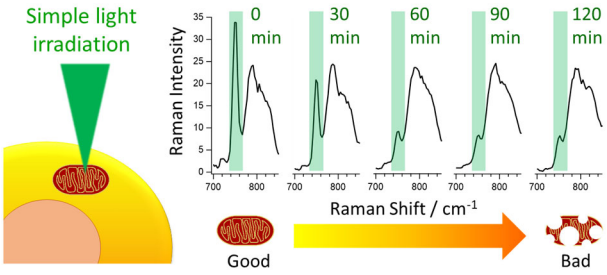

No pretreatment needed, totally label-free